


Article

AIPE-Active Neutral Ir(III) Complexes as Bi-Responsive Luminescent Chemosensors for Sensing Picric Acid and Fe³⁺ in Aqueous Media

Qinglong Zhang ^{1,†}, Jiangchao Xu ^{1,†}, Qiang Xu ^{2,*} and Chun Liu ^{1,*} 

- ¹ State Key Laboratory of Fine Chemicals, Frontier Science Center for Smart Materials, School of Chemical Engineering, Dalian University of Technology, Linggong Road 2, Dalian 116024, China; zhangqinglong@mail.dlut.edu.cn (Q.Z.); xujc@mail.dlut.edu.cn (J.X.)
- ² Instrumental Analysis Center, Dalian University of Technology, Dalian 116024, China
- * Correspondence: qiangxu@dlut.edu.cn (Q.X.); cliu@dlut.edu.cn (C.L.)
- † These authors contributed equally to this work.

Abstract: Three neutral iridium complexes **Ir1–Ir3** were synthesized using diphenylphosphoryl-substituted 2-phenylpyridine derivatives as the cyclometalating ligand and picolinic acid as the auxiliary ligand. They exhibited significant aggregation-induced phosphorescent emission (AIPE) properties in H₂O/THF and were successfully used as bi-responsive luminescent sensors for the detection of picric acid (PA) and Fe³⁺ in aqueous media. **Ir1–Ir3** possesses high efficiency and high selectivity for detecting PA and Fe³⁺, with the lowest limit of detection at 59 nM for PA and 390 nM for Fe³⁺. Additionally, the complexes can achieve naked-eye detection of Fe³⁺ in aqueous media. **Ir1–Ir3** exhibit excellent potential for practical applications in complicated environments. The detection mechanism for PA is attributed to photo-induced electron transfer (PET) and Förster resonance energy transfer (FRET), and the detection mechanism for Fe³⁺ may be explained by PET and the strong interactions between Fe³⁺ and the complexes.

Keywords: neutral iridium(III) complex; AIPE property; bi-responsive luminescent chemosensor; picric acid; Fe³⁺



Received: 8 December 2024
Revised: 3 January 2025
Accepted: 5 January 2025
Published: 8 January 2025

Citation: Zhang, Q.; Xu, J.; Xu, Q.; Liu, C. AIPE-Active Neutral Ir(III) Complexes as Bi-Responsive Luminescent Chemosensors for Sensing Picric Acid and Fe³⁺ in Aqueous Media. *Chemosensors* **2025**, *13*, 10. <https://doi.org/10.3390/chemosensors13010010>

Copyright: © 2025 by the authors. Licensee MDPI, Basel, Switzerland. This article is an open access article distributed under the terms and conditions of the Creative Commons Attribution (CC BY) license (<https://creativecommons.org/licenses/by/4.0/>).

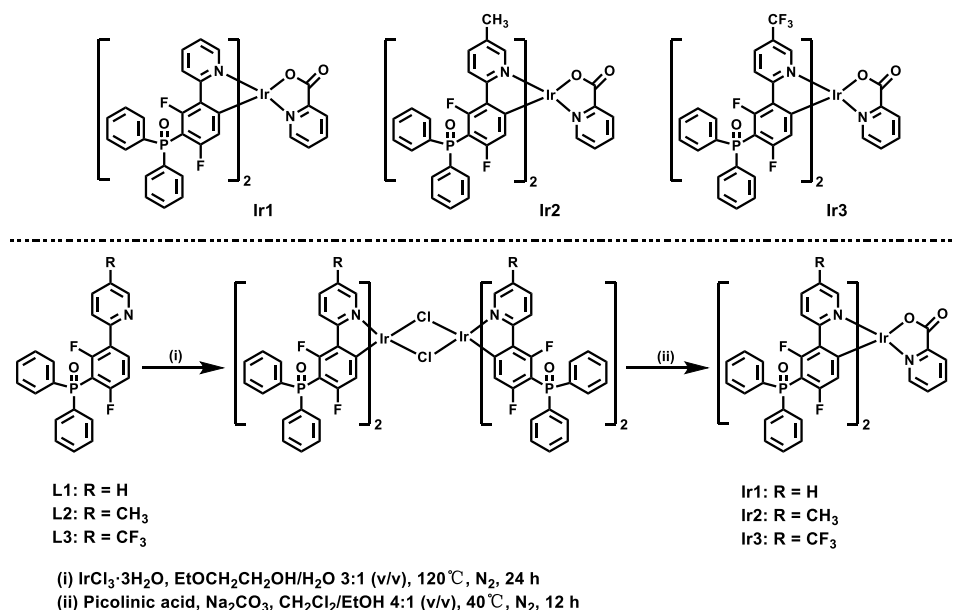
1. Introduction

The detection of trace explosives and heavy metal ions in the environment has attracted widespread attention from researchers out of concern for social security, human health, and environmental protection [1–3]. Compared with other nitro explosives, picric acid (PA) possesses stronger explosive properties and is a crucial component of military explosives [4]. In addition to its military applications, PA is also commonly used in the production of dyes, leather, and fireworks [5]. However, PA can cause serious environmental damage and human diseases such as skin irritation, liver function abnormalities, and cancer when it leaks into the environment [4,6]. Additionally, iron is a critical element in the body that plays a vital role in biochemical processes. The balance of Fe³⁺ is crucial for human health because its deficiency or over-accumulation can lead to various disorders of living system, including anemia, liver and kidney damage, organ failure, Parkinson's, Alzheimer's, and cancer [7–10]. Moreover, excessive Fe³⁺ can also cause severe environmental problems [11]. Therefore, the development of simple and efficient methods for the detection of PA and Fe³⁺ is highly urgent.

Luminescent sensing methods for detecting pollutants have garnered considerable attention due to their cost-effectiveness, simplicity, rapid response, and non-destructive nature compared to other techniques [12–14]. In recent years, iridium complexes have been widely applied in the luminescence sensing of various analytes due to their rich tunable photophysical properties and multifunctionality [15–18]. Furthermore, the concept of aggregation-induced phosphorescent emission (AIPE) has provided new approaches for iridium complexes to be used as chemosensors in aqueous media or solid-state, promoting their practical application in the environment [19–23].

A series of AIPE-active Ir(III) complexes have been successfully utilized for the detection of PA in aqueous media, exhibiting satisfactory sensing outcomes [24–27]. The luminescence quenching of most Ir(III) complexes is attributed to photo-induced electron transfer (PET) during the detection. However, Förster resonance energy transfer (FRET) has also been established as a significant quenching mechanism, and the presence of FRET can significantly improve the selectivity and quenching efficiency of Ir(III) complexes toward PA [28,29]. Based on the detection mechanism, the development of Ir(III) complexes that can achieve the synergistic effects of PET and FRET in detection is of great importance for the efficient and selective detection of PA. In addition, organic small molecules [11], metal–organic frameworks [30], coordination polymers [31], and nanoparticles [32] have been employed for detecting Fe^{3+} in previous studies. However, reports on the detection of Fe^{3+} by Ir(III) complexes in aqueous media are scarce to date [33]. To the best of our knowledge, there have been no reports of Ir(III) complexes performing bi-responsive detection of PA and Fe^{3+} in aqueous media.

Our group has long been committed to studying the structure-function relationship of cyclometalated metal complexes [34–40]. Recently, we have developed a series of cyclometalated Pt(II) and Ir(III) complexes for detecting PA in aqueous media by the detection mechanism of PET [34–38]. However, the impact of the structure of neutral Ir(III) complexes on their detection performance remains to be investigated. The diphenylphosphoryl group is a strong electron-withdrawing group, and its introduction at the corresponding positions of Ir(III) complexes can lower the highest occupied molecular orbital (HOMO), which leads to blue light emission from the Ir(III) complexes and enhances the FRET with the analyte [41,42]. Moreover, the oxygen atom in the diphenylphosphoryl group contributes to the specific recognition of metal ions [11,43,44]. Therefore, three neutral Ir(III) complexes **Ir1–Ir3** have been synthesized using diphenylphosphoryl-substituted 2-phenylpyridine derivatives as the cyclometalating ligand and picolinic acid as the auxiliary ligand. They exhibit significant AIPE properties in $\text{H}_2\text{O}/\text{THF}$. We successfully achieved efficient detection of PA and specific recognition of Fe^{3+} in aqueous media using their AIPE properties and discuss the possible detection mechanisms in detail. Moreover, **Ir1–Ir3** show promising practical applications in environmental water samples. The structures of **Ir1–Ir3** are shown in Scheme 1.



Scheme 1. Structures and the synthetic routes of **Ir1–Ir3**.

2. Materials and Methods

2.1. Materials and Instruments

Further details of the materials and instruments utilized for this study are in the Supplementary Materials.

2.2. Characterization of Complexes

The cyclometalating ligands and cyclometalated Ir(III) complexes **Ir1–Ir3** have been synthesized following the previously reported methods, and the detailed characterization results of **Ir1–Ir3** are in the Supplementary Materials Figures S1–S8 [45]. Scheme 1 shows the synthetic routes of **Ir1–Ir3**, and the detailed synthetic steps are illustrated as follows.

IrCl₃·3H₂O (0.2 mmol, 70.5 mg) and cyclometalating ligand (0.5 mmol) were added to 8 mL of 2-ethoxyethanol/water (3:1, v/v), which was heated at 120 °C for 24 h under a nitrogen atmosphere. After the reaction, the mixture was added to water, the resulting precipitate was filtered and washed with ethanol and *n*-hexane to obtain the chloro-bridged dimer. Without further purification, the dimer, picolinic acid (0.6 mmol, 73.9 mg), and Na₂CO₃ (1.0 mmol, 106.0 mg) were added to 5 mL of CH₂Cl₂/ethanol (4:1, v/v). The mixture was stirred at 40 °C for 12 h under N₂. After the reaction, the mixture was added to brine and extracted with CH₂Cl₂. With CH₂Cl₂/CH₃OH (10:1, v/v) as the eluent, the mixture was purified by silica gel column chromatography to obtain **Ir1–Ir3**.

2.3. Methods for Test of AIPE and Detection of PA and Fe³⁺

Stock solutions of **Ir1–Ir3** in THF (100 μM) were prepared. Subsequently, the suspensions of **Ir1–Ir3** (3 mL, 10 μM) at different water fractions were prepared by mixing 300 μL of the stock solution with THF and deionized water of appropriate volume, and their emission spectra were recorded. The suspensions of **Ir1–Ir3** (10 μM) in H₂O/THF with a 70% water fraction were prepared in a 200 mL volumetric flask, respectively, and 3 mL of the suspension was used for the measurement of emission and absorption spectra each time. PA solutions with concentrations from 0.1 to 40 mM and Fe(NO₃)₃ solutions at concentrations from 0 to 100 mM were prepared in H₂O/THF (v/v = 7:3), respectively. For the detection of PA or Fe³⁺ by **Ir1–Ir3**, PA or Fe(NO₃)₃ solutions (30 μL) with different concentrations were added to 3 mL of the suspensions of the complexes each time, and their emission and absorption spectra were recorded. For the selectivity experiments

with **Ir1–Ir3**, various analytes (20 mM, nitromethane (NM), *m*-dinitrobenzene (1,3-DNB), 4-methoxyphenol (MEHQ), nitrobenzene (NB), phenol, *p*-cresol, and *m*-cresol) and ionic compounds (20 mM, KF, KBr, NaHCO₃, CH₃COONa, FeCl₂, ZnCl₂, MgSO₄, CuSO₄, CaCl₂, MnCl₂, NiCl₂, and CoCO₃) were added to the suspensions of the complexes, and their emission spectra were tested. For anti-interference experiments with **Ir1–Ir3** for detecting PA, PA solutions (20 mM) were added to suspensions of complexes with different analytes and ionic compounds, respectively, and their emission spectra were tested. In addition, Fe(NO₃)₃ solutions (80 mM for **Ir1** and **Ir2** and 100 mM for **Ir3**) were added to suspensions of the complexes with different ionic compounds for the measurement of their emission spectra to investigate the anti-interference ability of **Ir1–Ir3** for the detection of Fe³⁺. In order to study the ability of **Ir1–Ir3** when applied in the environment, several environmental water samples (tap water, lake water, and rainwater from Dalian University of Technology and seawater from Qixianling in Dalian) were selected instead of deionized water to prepare suspensions of the complexes. Subsequently, PA solutions (20 mM) or Fe(NO₃)₃ solutions (80 mM for **Ir1** and **Ir2**, and 100 mM for **Ir3**) were added to the suspensions of **Ir1–Ir3**, respectively, and their emission spectra were recorded.

WARNING! The nitroaromatic compounds used in optical measurement are highly explosive and should be handled safely and in small quantities.

3. Results and Discussion

3.1. Photophysical Properties

The UV–vis absorption spectra and normalized emission spectra of **Ir1–Ir3** in THF are shown in Figure 1a,b, and the detailed photophysical data are listed in Table S1. As shown in Figure 1a, the UV–vis absorption spectra of **Ir1–Ir3** are similar to those of previously reported Ir(III) complexes, with intense absorptions at 200–350 nm, which are mainly attributed to spin-allowed ligand-centered (¹π–π*) transitions. The weaker absorptions within 350 to 500 nm can be assigned to the combination of metal-to-ligand charge transfer (¹MLCT and ³MLCT) with ligand-centered ³π–π* transitions [21,38]. The normalized emission spectra of **Ir1–Ir3** in THF are shown in Figure 1b. The results show that the introduction of a methyl group onto the cyclometalating ligand leads to a slight redshift of 3 nm for **Ir2** compared to non-substituted **Ir1**, while the introduction of a trifluoromethyl group for **Ir3** leads to a larger redshift of 28 nm relative to **Ir1**. In addition, **Ir1** and **Ir2** exhibit vibronic fine structure, suggesting a large ligand-centered (C[∞]N) character (³LC). Unlike **Ir1** and ³Ir2, the featureless emission spectrum of **Ir3** may be attributed to more ³MLCT/³LLCT features contained in **Ir3** [20,24,26]. **Ir1–Ir3** exhibit high phosphorescence quantum yields (Φ_{PL}) in deoxygenated CH₂Cl₂, which are estimated to be 0.69, 0.70, and 0.72, respectively (Table S1). The lifetimes (τ) of **Ir1–Ir3** in degassed CH₂Cl₂ are estimated to be 1.32, 3.32, and 1.01 μs, respectively, at room temperature (Figure S9 and Table S1). This indicates that substituents on the cyclometalating ligand can significantly affect the excited-state properties of **Ir2** and **Ir3**, leading to variations in their lifetimes. The data demonstrate that substituents on the cyclometalating ligand play an essential role in the modification of the photophysical properties of the Ir(III) complexes.

3.2. AIPE Properties

Multiple rotatable phenyl groups are present in **Ir1–Ir3** due to the introduction of the diphenylphosphoryl group, which motivates us to investigate their AIPE properties. The emission spectra of **Ir1–Ir3** in H₂O/THF are shown in Figure 2a–c. Below a 70% water fraction, the emission intensities of **Ir1–Ir3** increase continuously with increasing water fraction and reach the maximum at 70% water fraction, showing obvious AIPE properties. Dynamic light scattering (DLS) experiments were carried out in the case of **Ir1** (Figure S10).

The results indicate that **Ir1** forms aggregates at 70%, 80%, and 90% water fractions, with hydrodynamic diameters of 208, 259, and 222 nm, respectively. In the aggregated state, the motion of the freely rotatable phenyl groups in the cyclometalating ligand of the complex is restricted, which inhibits the non-radiative pathway, thus allowing the excitons to return to the ground state by radiative pathway and leading to significant AIPE activity.

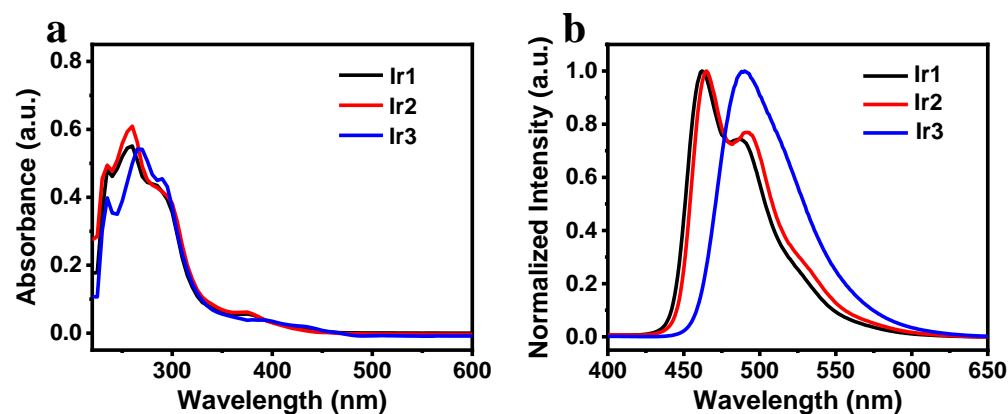


Figure 1. The UV-vis absorption spectra (a) and normalized emission spectra (b) of **Ir1–Ir3** at room temperature (10 μ M in THF). The excitation wavelength was 330 nm.

3.3. Sensing of PA

The AIPE phenomenon exhibited by **Ir1–Ir3** in H_2O/THF prompted us to use them for the detection of PA in aqueous media. The good photostability of **Ir1–Ir3** in H_2O/THF ($v/v = 7:3$) was determined first (Figure S11). Subsequently, luminescence response experiments of the complexes to PA were conducted by adding PA solutions at different concentrations to suspensions of **Ir1–Ir3**. The emission intensities of the complexes decrease continuously with increasing PA concentration (Figure 3a–c). The quenching efficiencies of **Ir1–Ir3** at a PA concentration of 10 μ M (1 equiv.) are 23.3%, 23.0%, and 16.8%, respectively. With increasing PA concentrations up to 200 μ M (20 equiv.), the quenching efficiencies of **Ir1–Ir3** reach 97.4%, 96.0%, and 93.1%, respectively, and their emission intensities are negligible (Figure S12).

The phosphorescence response effect of the complex to PA can be studied utilizing the Stern–Volmer (SV) plot, which is constructed from the emission intensity ratio I_0/I (I_0 is the emission intensity in the absence of PA, and I is the emission intensity in the presence of PA) versus the concentration of PA, as shown in Figure 3d–f. The SV plots of **Ir1–Ir3** show a good linear relationship at PA concentration from 0 to 10 μ M, whereas the plots gradually deviate from the linearity and the luminescence quenching effects become stronger with the increase of PA concentration. At PA concentration from 0 to 10 μ M, the quenching constant (K_{SV}) can be determined by the SV equation: $I_0/I = K_{SV} [Q] + 1$ [46], which represents the sensitivity of the complex to detect PA. The K_{SV} of **Ir1–Ir3** is estimated to be 3.1×10^4 , 3.0×10^4 , and 2.0×10^4 M^{-1} , respectively, indicating the high sensitivity of the complexes for the detection of PA. Additionally, the LODs of **Ir1–Ir3** are estimated at 59, 84, and 95 nM, respectively, according to the limit of detection (LOD) equation: $LOD = 3\sigma/K$ (Table S2 and Figure S13) [47]. The results indicate that **Ir1–Ir3** are promising for the efficient detection of PA in aqueous media.

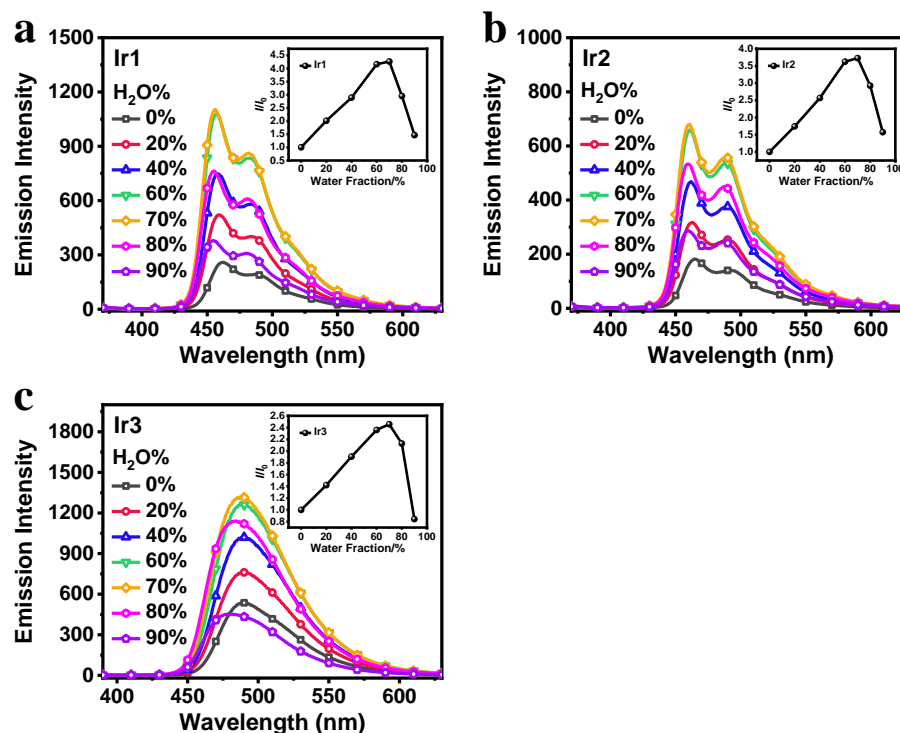


Figure 2. Emission spectra of Ir1 (a), Ir2 (b), and Ir3 (c) in H₂O/THF with different water fractions ($c = 10 \mu\text{M}$, $\lambda_{\text{ex}} = 330 \text{ nm}$). Insert: The relationship between the relative emission intensity I/I_0 (I is the maximum emission intensity in H₂O/THF and I_0 is the maximum emission intensity in THF) of Ir1–Ir3 and different water fractions.

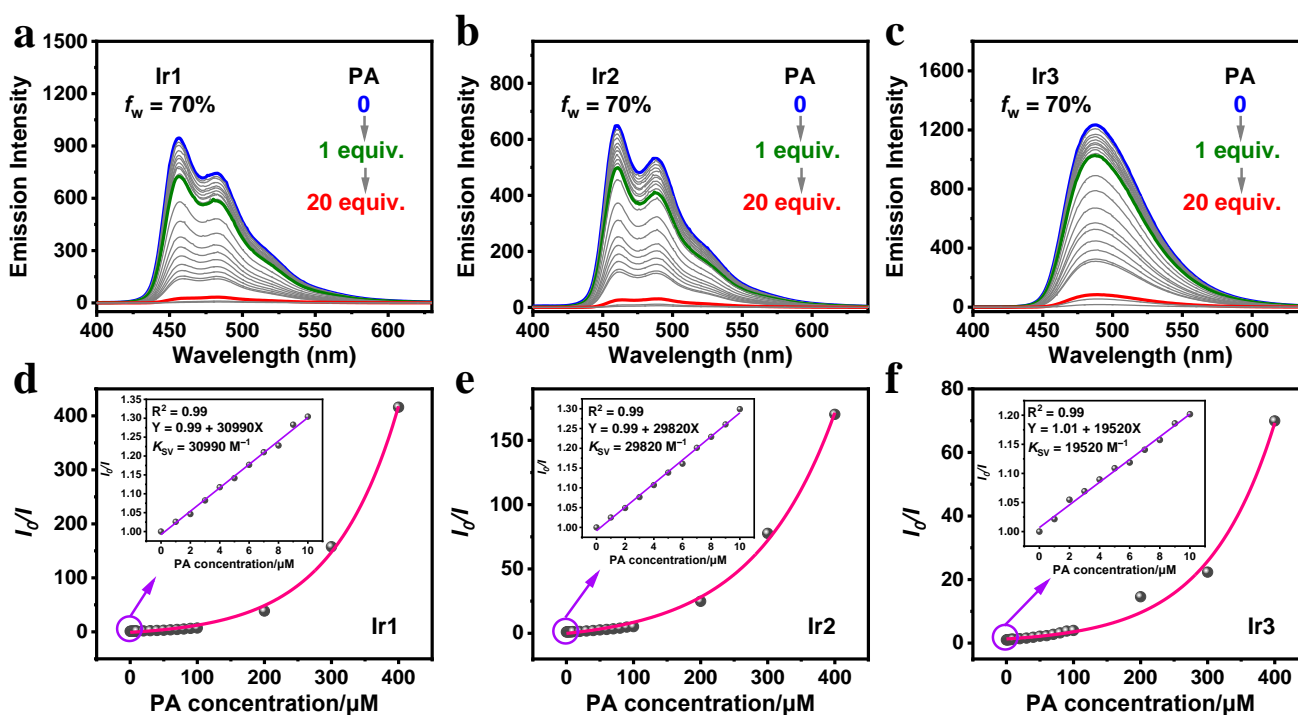


Figure 3. The emission spectra of Ir1 (a), Ir2 (b), and Ir3 (c) in H₂O/THF ($v/v = 7:3$, $10 \mu\text{M}$) with PA at different concentrations. The excitation wavelength was 330 nm. The Stern–Volmer plots of Ir1 (d), Ir2 (e), and Ir3 (f) for PA. Insert: Linear SV plots of Ir1–Ir3 at PA concentrations from 0 to 10 μM.

Considering the complexity of the probe in practical application, the selectivity, anti-interference properties, and applicability in environmental water samples of Ir1–Ir3 were explored.

Firstly, a variety of analytes (NM, 1,3-DNB, MEHQ, NB, phenol, *p*-cresol, and *m*-cresol) and ionic compounds (KF, KBr, NaHCO₃, CH₃COONa, FeCl₂, ZnCl₂, MgSO₄, CuSO₄, CaCl₂, MnCl₂, NiCl₂, and CoCO₃) were utilized to perform selectivity and anti-interference experiments. As shown in Figures 4a,b, S14a,b, and S15a,b, the addition of analytes and ionic compounds (20 equiv.) has minimal effect on the emission intensities of Ir1–Ir3, and the quenching efficiencies are all less than 20%, which are much lower than the quenching efficiencies of the complexes for PA. Thus, the results suggest that the luminescence of Ir1–Ir3 can be selectively quenched by PA. Subsequently, PA solutions (20 equiv.) were added to the suspensions of Ir1–Ir3 in the presence of various analytes and ionic compounds for anti-interference experiments. The results indicate that the luminescence of Ir1–Ir3 in the presence of other analytes and ionic compounds can still be quenched effectively by PA, and the quenching efficiencies are almost the same as those in the presence of PA only (Figures 4c,d, S14c,d, and S15c,d). The presence of various analytes and ionic compounds has almost no effect on the performance in detecting PA by the complexes. Therefore, Ir1–Ir3 exhibit excellent selectivity and anti-interference ability to detect PA in aqueous media.

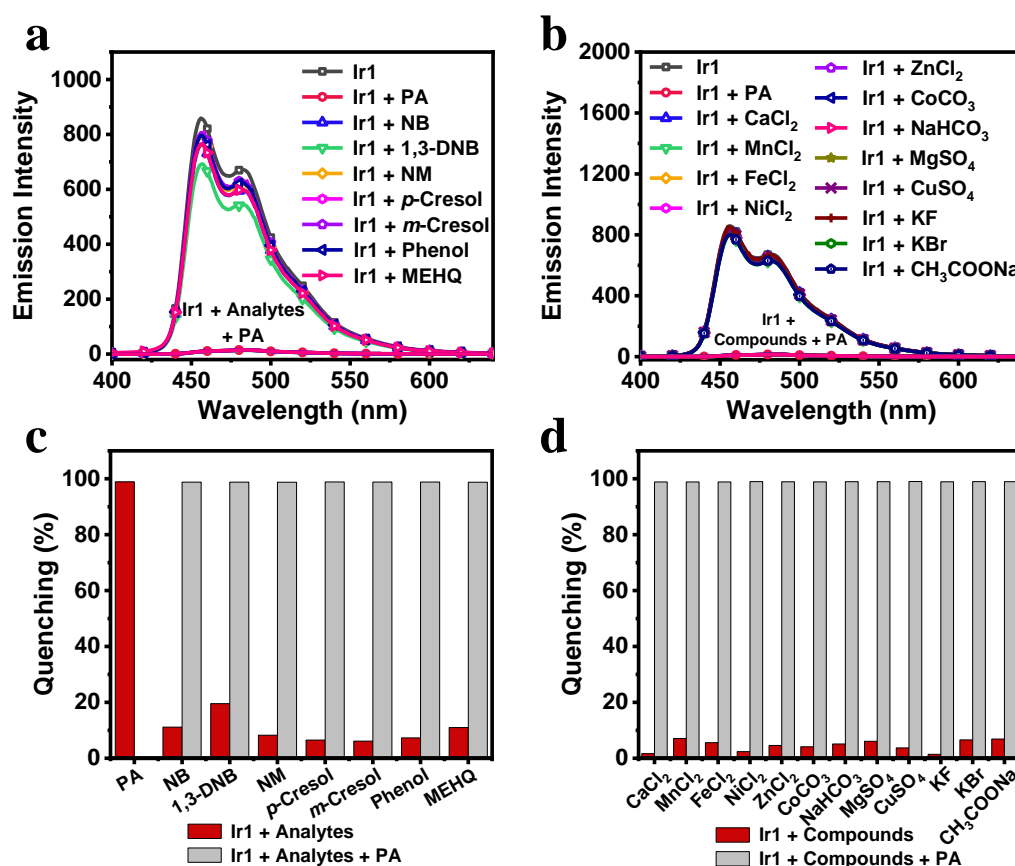


Figure 4. The emission spectra of Ir1 in H₂O/THF (*v/v* = 7:3, 10 μM) with different analytes (a) and ionic compounds (b). The excitation wavelength was 330 nm. Quenching percentages of Ir1 with different analytes (c) and ionic compounds (d) before (red) and after (gray) the addition of PA.

To investigate the applicability of Ir1–Ir3 for the detection of PA in real environments, luminescence quenching experiments of these complexes for PA were conducted in H₂O/THF, utilizing tap water, lake water, seawater, and rainwater instead of deionized water. As shown in Figure 5a–c, the emission spectra of Ir1–Ir3 in different water samples are almost the same as those in deionized water, indicating that the complexes have good stability in various environmental water samples. Moreover, the luminescence of Ir1–Ir3 in

different water samples can be effectively quenched by PA with almost the same quenching efficiencies (Figure 5d). The results indicate that the complexes are promising for efficient and selective detection of PA in real environments.

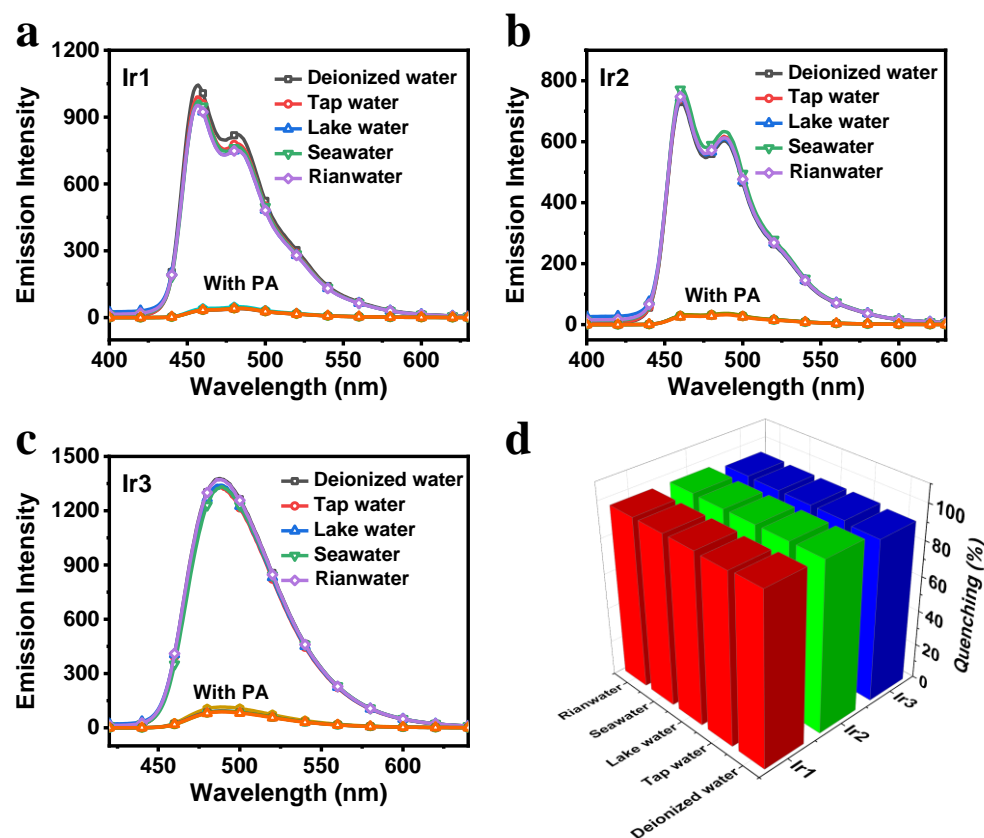


Figure 5. The luminescent response of Ir1 (a), Ir2 (b), and Ir3 (c) toward PA in several environmental water samples ($c = 10 \mu\text{M}$, $\lambda_{\text{ex}} = 330 \text{ nm}$). (d) Quenching percentage of Ir1–Ir3 towards PA in environmental water samples.

3.4. Sensing of Fe^{3+}

To achieve naked-eye detection of Fe^{3+} by the complexes, Fe^{3+} solutions were added to the suspensions of Ir1–Ir3 to observe the color change. As shown in Figures S16, S17a, and S18a, the colors of suspensions of Ir1–Ir3 gradually change from colorless to light yellow within 10 min after adding Fe^{3+} at different concentrations, which indicates that the possible interaction between Fe^{3+} and complexes leads to the color change. Subsequently, the selectivity of the complexes for the detection of Fe^{3+} was investigated by adding various ionic compounds to the suspensions of Ir1–Ir3 and monitoring the resulting color changes (Figures 6, S17b and S18b). The results show that only the color of the suspension of Ir1–Ir3 in the presence of Fe^{3+} changes to light yellow, while the color of the suspensions with other ions does not change. Therefore, the complexes are specific for the naked-eye detection of Fe^{3+} .

Subsequently, luminescence quenching experiments were conducted by adding Fe^{3+} solutions of different concentrations to suspensions of Ir1–Ir3. Similar to the luminescence quenching phenomenon in the detection of PA by the complexes, the emission intensities of Ir1–Ir3 decrease with increasing Fe^{3+} concentration (Figure 7a–c). When the concentration of Fe^{3+} is $70 \mu\text{M}$ (7 equiv.), the quenching efficiencies of Ir1–Ir3 are 24.5%, 27.2%, and 22.7%, respectively. As the Fe^{3+} concentration reaches $800 \mu\text{M}$ (80 equiv.), the quenching efficiencies of Ir1 and Ir2 are 94.8% and 94.4%, respectively, while at a Fe^{3+} concentration of

1000 μM (100 equiv.), the quenching efficiency of **Ir3** reaches 90.3%, and their luminescence is almost completely quenched (Figure S19).

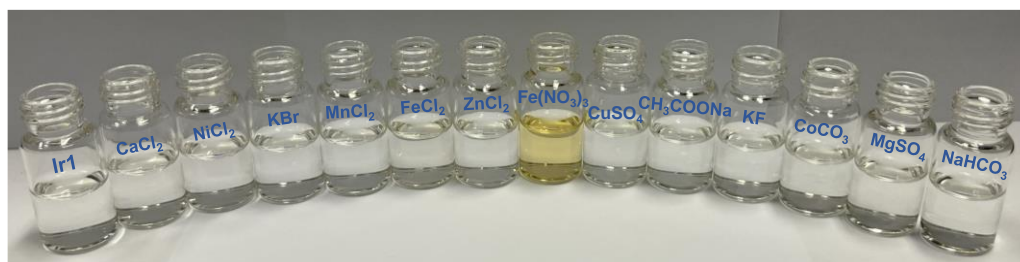


Figure 6. The color of **Ir1** in $\text{H}_2\text{O}/\text{THF}$ in the presence of various ionic compounds.

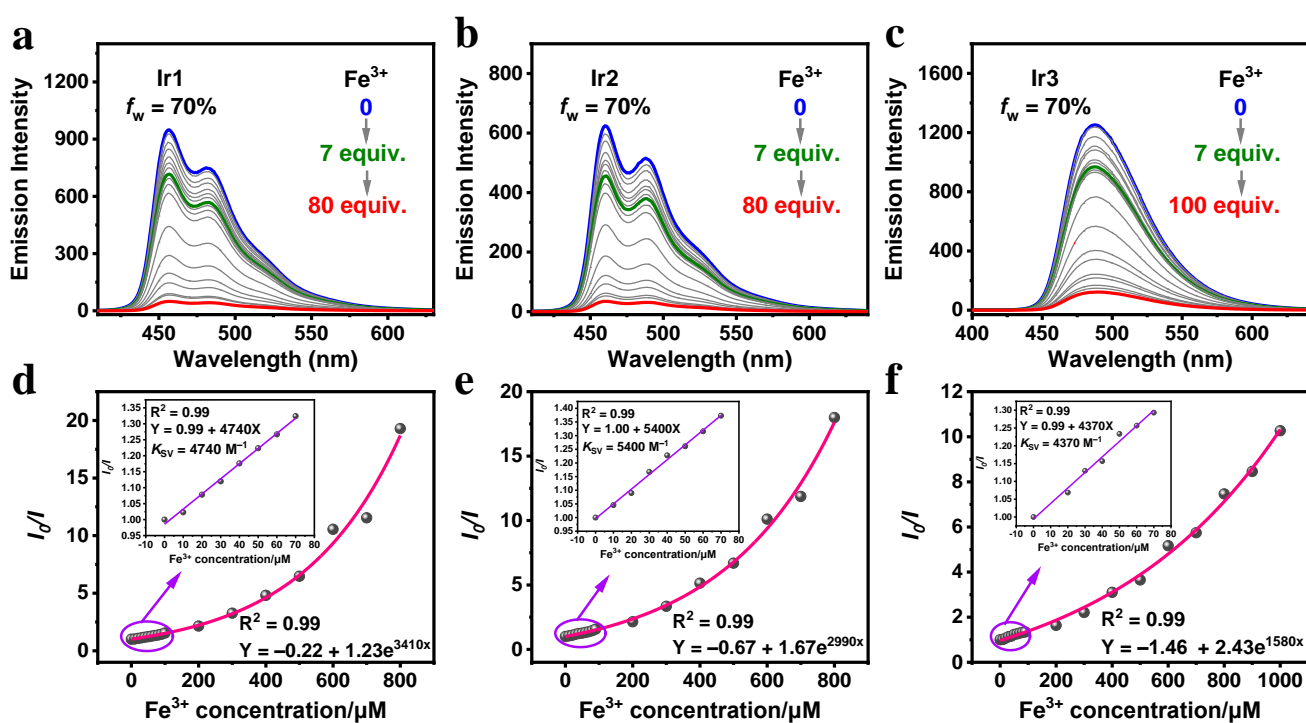


Figure 7. The emission spectra of **Ir1** (a), **Ir2** (b), and **Ir3** (c) in $\text{H}_2\text{O}/\text{THF}$ ($v/v = 7:3$, 10 μM) with Fe^{3+} at different concentrations. The excitation wavelength was 330 nm. The Stern–Volmer plots of **Ir1** (d), **Ir2** (e), and **Ir3** (f) for Fe^{3+} . Inset: Linear SV plots of **Ir1**–**Ir3** at Fe^{3+} concentrations from 0 to 70 μM .

The SV plots are constructed using the emission intensity ratio I_0/I versus Fe^{3+} concentration, as shown in Figure 7d–f. At a Fe^{3+} concentration of 0–70 μM , the SV plots of **Ir1**–**Ir3** show good linear relationships, whereas the plots gradually deviate from linearity and the luminescence quenching effects gradually become stronger with the increase of Fe^{3+} concentration. In the range of a Fe^{3+} concentration of 0–70 μM , the values of K_{SV} for **Ir1**–**Ir3** estimated by the SV equation are 4740, 5400, and 4370 M^{-1} , respectively. These values suggest that the complexes exhibit high sensitivity for the detection of Fe^{3+} . In addition, the LODs of **Ir1**–**Ir3** for Fe^{3+} are estimated at 390, 510, and 450 nM, respectively, according to the LOD equation (Table S2 and Figure S20). Therefore, **Ir1**–**Ir3** are promising for detecting Fe^{3+} efficiently in aqueous media.

Similarly, the selectivity, anti-interference properties, and environmental applicability of **Ir1**–**Ir3** in the detection of Fe^{3+} were explored. It was demonstrated in the section on sensing of PA that various ionic compounds have minor effects on the emission spectra of **Ir1**–**Ir3**, suggesting that **Ir1**–**Ir3** possess the ability to specifically recognize Fe^{3+} (Figures 4b, S14b and S15b). Subsequently, Fe^{3+} solutions were added to the suspensions

of **Ir1–Ir3** with various ions present, and their emission spectra were measured, as shown in Figure 8a–c. The luminescence of the complexes can still be effectively quenched by Fe^{3+} in the presence of various ions, and the quenching efficiencies are almost the same as those with only Fe^{3+} present (Figure 8d). The results demonstrate that **Ir1–Ir3** exhibit good selectivity and anti-interference in the detection of Fe^{3+} .

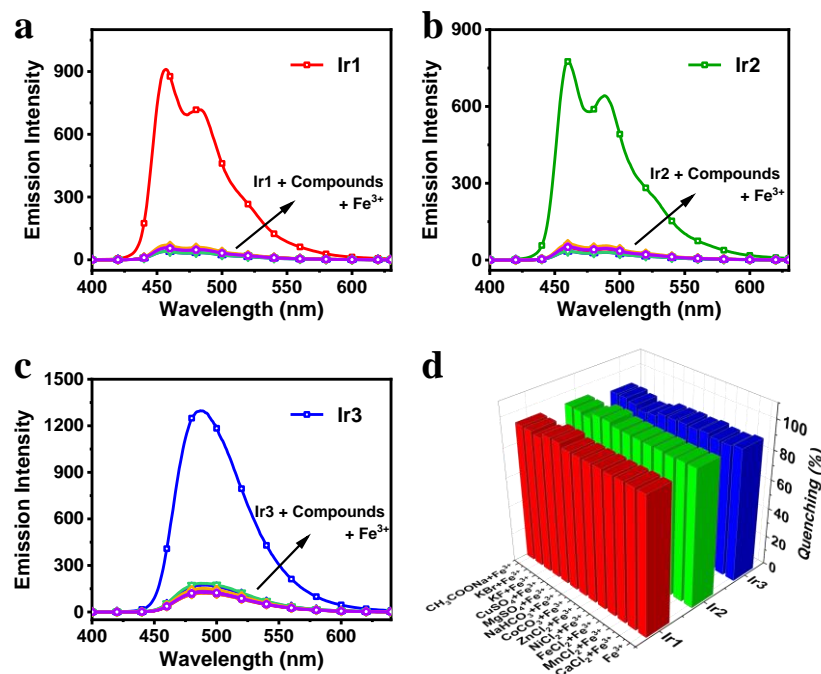


Figure 8. The emission spectra of **Ir1** (a), **Ir2** (b), and **Ir3** (c) in $\text{H}_2\text{O}/\text{THF}$ ($v/v = 7:3$, $10 \mu\text{M}$) in the simultaneous presence of other ionic compounds and Fe^{3+} . The excitation wavelength was 330 nm. (d) Quenching percentages of **Ir1–Ir3** in the simultaneous presence of other ionic compounds and Fe^{3+} .

To study the applicability of **Ir1–Ir3** for the detection of Fe^{3+} in real environments, luminescence quenching experiments of the complexes for Fe^{3+} were performed in different environmental water samples. As shown in Figure 9a–c, the luminescence of **Ir1–Ir3** in different water samples is effectively quenched by Fe^{3+} , with nearly identical quenching efficiencies (Figure 9d), suggesting that these complexes possess the potential to detect Fe^{3+} efficiently and highly selectively in the environment.

3.5. Sensing Mechanism

The luminescence quenching process usually consists of dynamic quenching and static quenching, and the key to distinguishing between these two processes is whether the lifetime of the luminescence sensor is changed by the addition of analytes [48]. Therefore, the lifetime decay traces were measured after adding PA at different concentrations to the suspensions of **Ir1** (Figure 10a) and were fitted with computer software (Fluoracle, version 2.17.2) to obtain the lifetimes of **Ir1**. As shown in Figure S21, the lifetime of **Ir1** decreases with the increase in PA concentration, which indicates that there are dynamic quenching processes in the luminescence quenching of **Ir1** for PA. Subsequently, the UV–vis absorption spectra of **Ir1** with PA at different concentrations were tested, as shown in Figure 10b. The addition of PA only leads to the increase in the absorbance for **Ir1** at 225 and 250 nm, whereas there is no significant change in the shape and position of the absorption peaks. The increasing absorption peak appearing at 360 nm is attributed to the increasing concentration of PA. Therefore, there is no static quenching process in the luminescence quenching of **Ir1** for PA.

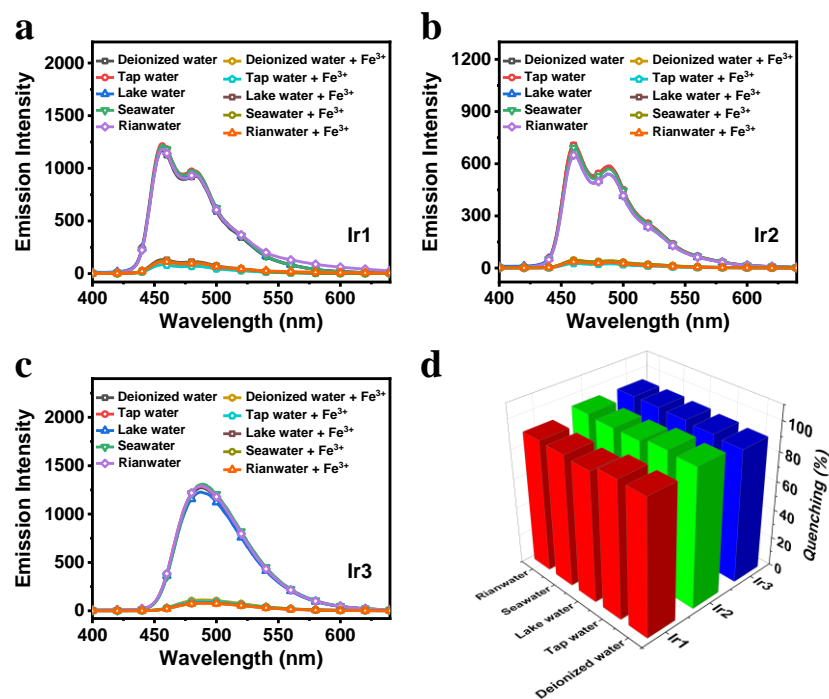


Figure 9. The luminescent response of Ir1 (a), Ir2 (b), and Ir3 (c) toward Fe^{3+} in several environmental water samples ($c = 10 \mu\text{M}$, $\lambda_{\text{ex}} = 330 \text{ nm}$). (d) Quenching percentage of Ir1–Ir3 toward Fe^{3+} in environmental water samples.

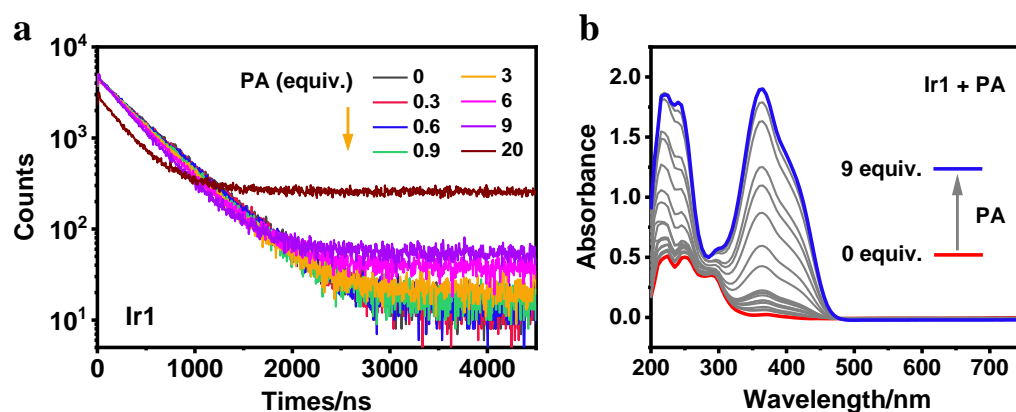


Figure 10. (a) Phosphorescence decay traces of Ir1 in $\text{H}_2\text{O}/\text{THF}$ ($v/v = 7:3$, $10 \mu\text{M}$) with PA at various concentrations present. (b) UV-vis absorption spectra of Ir1 in $\text{H}_2\text{O}/\text{THF}$ with PA at different concentrations.

In order to better understand the dynamic quenching process of Ir1 for PA, density functional theory (DFT) calculations were performed for Ir1, PA, and their adduct (Ir1 + PA) to determine the presence or absence of PET in the detection process, as shown in Figure 11a. The LUMO energy of Ir1 is higher than that of PA, and thus the excited state electrons of Ir1 will be transferred from the LOMO of Ir1 to that of PA and will not return to the HOMO of Ir1, and thus the luminescence of Ir1 will be quenched. In addition, the adduct has the highest stability because of its lowest energy gap. The results indicate the existence of the PET process in the luminescence quenching of Ir1 for PA. Furthermore, there is a partial overlap between the emission spectrum of Ir1 and the absorption spectrum of PA, suggesting the presence of FRET during luminescence quenching (Figure 11b). Therefore, the luminescence quenching of Ir1 for PA is the result of the synergistic effect of PET and FRET, which leads to the high efficiency and selectivity of Ir1 for detecting PA. In addition, the Job's plot was obtained by measuring the emission spectra of the mixed systems at the

different molar fractions of **Ir1** while keeping the total concentration of **Ir1** and PA constant (10 μM). As shown in Figure 12, the intersection in the Job's plot is observed at the molar fraction of **Ir1** of 0.5, indicating that the stoichiometric ratio of **Ir1** toward PA is 1:1 [49].

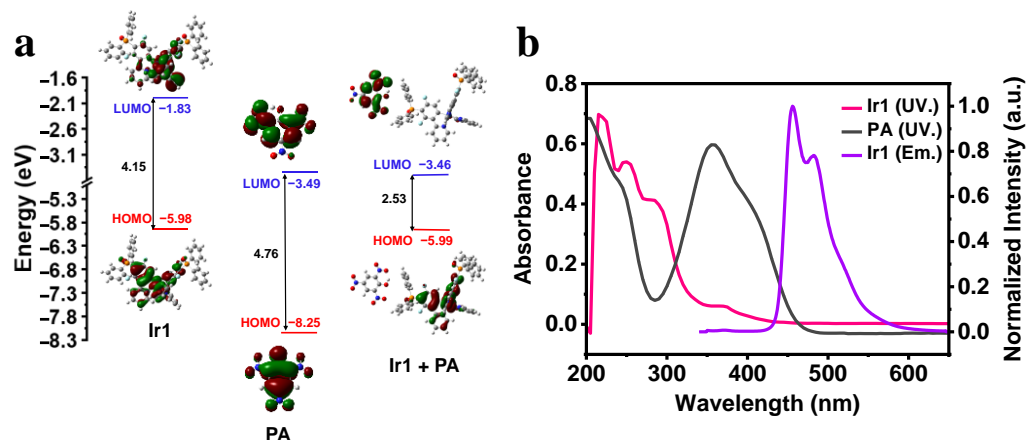


Figure 11. (a) Calculated energy level diagram of **Ir1**, PA, and adduct (**Ir1** + PA). (b) UV-vis absorption spectra of **Ir1** (pink) and PA (black), and normalized emission spectrum of **Ir1** (purple) ($\lambda_{\text{ex}} = 330 \text{ nm}$).

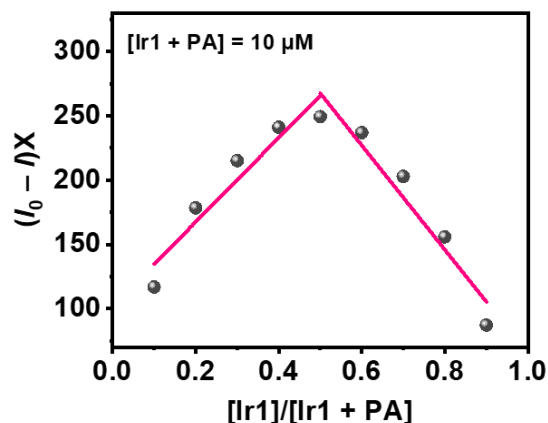


Figure 12. Job's plot of **Ir1** with PA obtained by emission spectra measurements.

Similarly, the lifetime decay traces of **Ir1** in the presence of Fe^{3+} at different concentrations were tested (Figure 13a). The results indicate that the presence of Fe^{3+} also significantly reduces the luminescence lifetime of **Ir1**, suggesting that the dynamic quenching process occurs during the detection of Fe^{3+} (Figure S22). The absorption spectrum of Fe^{3+} does not overlap with the emission spectrum of **Ir1**, indicating the absence of FRET in detecting Fe^{3+} (Figure 13b). Thus, PET may be a reason for the luminescence quenching of **Ir1** in response to Fe^{3+} .

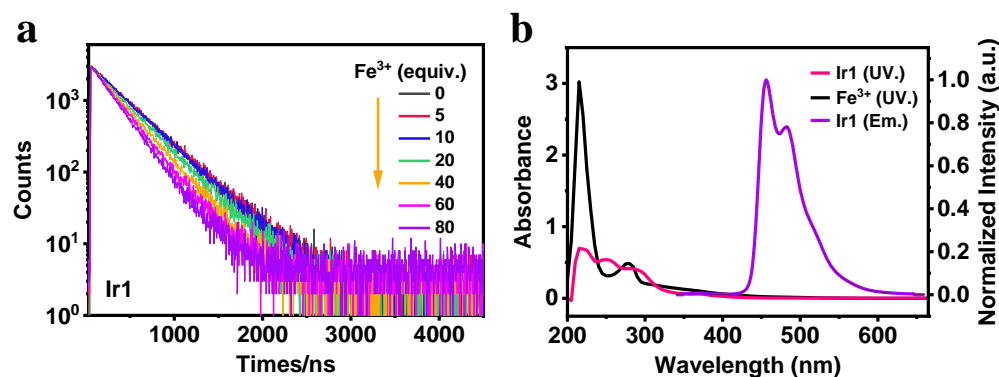


Figure 13. (a) Phosphorescence decay traces of **Ir1** in H₂O/THF (*v/v* = 7:3, 10 μM) with Fe³⁺ at various concentrations present. (b) UV–vis absorption spectra of **Ir1** (pink) and Fe³⁺ (black), and normalized emission spectrum of **Ir1** (purple) (λ_{ex} = 330 nm).

In addition, the UV–vis absorption spectra of **Ir1** with the addition of Fe³⁺ at different concentrations were tested, and the results are shown in Figure 14a. With the increase in Fe³⁺ concentration, the absorption peak of **Ir1** at 245 nm gradually disappears, while the absorption peak of **Ir1** at 225 nm gradually enhances and red-shifts to 245 nm. The absorption peaks of **Ir1** within the range of 200–250 nm change significantly with the addition of Fe³⁺, suggesting the existence of a static quenching process in the luminescence quenching of **Ir1** for Fe³⁺. This static quenching may arise from the interactions between Fe³⁺ and the oxygen atoms at the diphenylphosphoryl group of the cyclometalating ligand [11,44,50,51]. Thus, the luminescence quenching of **Ir1** for Fe³⁺ may be the result of a joint action of PET and static quenching. Additionally, the Job's plot of **Ir1** and Fe³⁺ are constructed and the intersection is noted at the molar fraction of **Ir1** of 0.5 (Figure 14b). Consequently, the results indicate that the stoichiometric ratio of **Ir1** toward Fe³⁺ is 1:1.

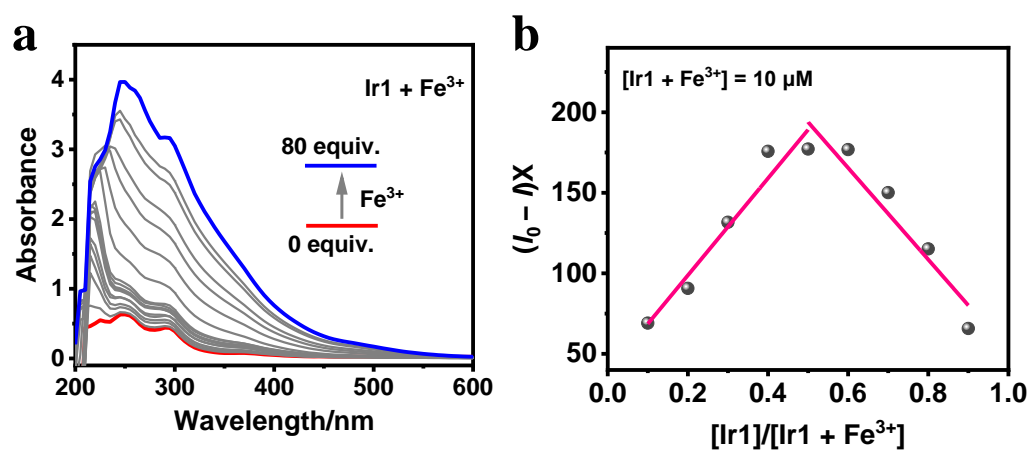


Figure 14. (a) UV–vis absorption spectra of **Ir1** in H₂O/THF with Fe³⁺ at different concentrations. (b) Job's plot of **Ir1** with Fe³⁺ obtained by emission spectra measurements.

4. Conclusions

In conclusion, three AIPE-active neutral Ir(III) complexes **Ir1–Ir3** were synthesized and successfully utilized as bi-responsive luminescent sensors for the detection of PA and Fe³⁺, respectively. All complexes provide efficient and selective detection of PA and Fe³⁺ in aqueous media. The quenching constants of **Ir1–Ir3** for PA are 3.1×10^4 , 3.0×10^4 , and 2.0×10^4 M^{−1}, respectively, and their LODs for PA are 59, 84, and 95 nM, respectively. The complexes also allow for naked-eye detection of Fe³⁺, which provides a more simplified method of Fe³⁺ detection. In addition, the quenching constants of **Ir1–Ir3** for Fe³⁺ are 4740, 5400, and 4370 M^{−1}, respectively, and their LODs for Fe³⁺ are 390, 510, and 450 nM,

respectively. **Ir1–Ir3** perform well in the detection of PA and Fe^{3+} in environmental water samples, thus promising to realize their applications in real environments. The detection mechanism of PA is attributed to the synergistic effect of PET and FRET, whereas the detection of Fe^{3+} may result from the joint action of PET and static quenching. These studies provide useful insights into the development and application of luminescent probes for multifunctional Ir(III) complexes.

Supplementary Materials: The following supporting information can be downloaded at: <https://www.mdpi.com/article/10.3390/chemosensors13010010/s1>, Figure S1: The ^1H NMR spectrum of **Ir1** in CDCl_3 ; Figure S2: The HRMS of **Ir1**. Inset: Theoretical (top) and high-resolution mass spectra (bottom) of **Ir1**; Figure S3: The ^1H NMR spectrum of **Ir2** in CDCl_3 ; Figure S4: The ^{13}C NMR spectrum of **Ir2** in CDCl_3 ; Figure S5: The HRMS of **Ir2**. Inset: Theoretical (left) and high-resolution mass spectra (right) of **Ir2**; Figure S6: The ^1H NMR spectrum of **Ir3** in CDCl_3 ; Figure S7: The ^{13}C NMR spectrum of **Ir3** in CDCl_3 ; Figure S8: The HRMS of **Ir3**. Inset: Theoretical (top) and high-resolution mass spectra (bottom) of **Ir3**; Figure S9: Phosphorescence decay profiles of **Ir1–Ir3** in deoxygenated CH_2Cl_2 ; Figure S10: DLS analysis of **Ir1** at 70% (a), 80% (b), and 90% (c) water fractions (10 μM , $\text{H}_2\text{O}/\text{THF}$); Figure S11: The emission spectra of **Ir1** (a), **Ir2** (b), and **Ir3** (c) in $\text{H}_2\text{O}/\text{THF}$ ($v/v = 7:3$, 10 μM) at eleven time points (blank measurement). The excitation wavelength was 330 nm; Figure S12: Quenching percentages of **Ir1** (a), **Ir2** (b), and **Ir3** (c) after adding PA at various concentrations. Inset: Photos of **Ir1–Ir3** at PA concentrations of 0 and 200 μM under 365 nm UV light; Figure S13: The linear graphs of the emission intensities of **Ir1** (a), **Ir2** (b), and **Ir3** (c) vs. the concentration of PA; Figure S14: The emission spectra of **Ir2** in $\text{H}_2\text{O}/\text{THF}$ ($v/v = 7:3$, 10 μM) with different analytes (a) and ionic compounds (b) present. The excitation wavelength is 330 nm. Quenching percentages of **Ir2** with different analytes (c) and ionic compounds (d) before (red) and after (gray) the addition of PA; Figure S15: The emission spectra of **Ir3** in $\text{H}_2\text{O}/\text{THF}$ ($v/v = 7:3$, 10 μM) with different analytes (a) and ionic compounds (b) present. The excitation wavelength is 330 nm. Quenching percentages of **Ir3** with different analytes (c) and ionic compounds (d) before (red) and after (gray) the addition of PA; Figure S16: The color change in **Ir1** in $\text{H}_2\text{O}/\text{THF}$ in the presence of Fe^{3+} at different concentrations. The Fe^{3+} concentrations are 0, 50, 100, 200, 300, 400, 500, 600, 700, and 800 μM from left to right, respectively; Figure S17: (a) The color change in **Ir2** in $\text{H}_2\text{O}/\text{THF}$ in the presence of Fe^{3+} at different concentrations. The Fe^{3+} concentrations are 0, 50, 100, 200, 300, 400, 500, 600, 700, and 800 μM from left to right, respectively. (b) The color of **Ir2** in $\text{H}_2\text{O}/\text{THF}$ in the presence of various ionic compounds; Figure S18: (a) The color change in **Ir3** in $\text{H}_2\text{O}/\text{THF}$ in the presence of Fe^{3+} at different concentrations. The Fe^{3+} concentrations are 0, 50, 100, 200, 300, 400, 500, 600, 700, and 800 μM from left to right, respectively. (b) The color of **Ir3** in $\text{H}_2\text{O}/\text{THF}$ in the presence of various ionic compounds. Figure S19: Quenching percentages of **Ir1** (a), **Ir2** (b), and **Ir3** (c) after adding Fe^{3+} at various concentrations; Figure S20: The linear graphs of the emission intensities of **Ir1** (a), **Ir2** (b), and **Ir3** (c) vs. the concentration of Fe^{3+} ; Figure S21: Lifetimes of **Ir1** in $\text{H}_2\text{O}/\text{THF}$ ($v/v = 7:3$, 10 μM) after the addition of PA at different concentrations; Figure S22: Lifetimes of **Ir1** in $\text{H}_2\text{O}/\text{THF}$ ($v/v = 7:3$, 10 μM) after the addition of Fe^{3+} at different concentration; Table S1. Photophysical data of **Ir1–Ir3**; Table S2. The emission intensities of **Ir1** at 456 nm, **Ir2** at 461 nm, and **Ir3** at 488 nm at eleven time points in $\text{H}_2\text{O}/\text{THF}$ ($v/v = 7:3$, 10 μM).

Author Contributions: Investigation, Q.Z. and J.X.; Data curation, Visualization, Writing—original draft, Q.Z.; Formal analysis, J.X.; Writing—review and editing, J.X., Q.X. and C.L.; Resources, Q.X. and C.L.; Funding acquisition, Supervision, C.L. All authors have read and agreed to the published version of the manuscript.

Funding: The authors thank the financial support from the National Natural Science Foundation of China (21978042) and the Fundamental Research Funds for the Central Universities (DUT22LAB610).

Institutional Review Board Statement: Not applicable.

Informed Consent Statement: Not applicable.

Data Availability Statement: Data are contained within the article.

Conflicts of Interest: The authors declare no conflicts of interest.

References

1. Cheng, T.; Hu, J.; Zhou, C.; Wang, Y.; Zhang, M. Luminescent metal-organic frameworks for nitro explosives detection. *Sci. China Chem.* **2016**, *59*, 929–947. [[CrossRef](#)]
2. Taniya, O.S.; Khasanov, A.F.; Sadieva, L.K.; Santra, S.; Nikonov, I.L.; Al-Ithawi, W.K.A.; Kovalev, I.S.; Kopchuk, D.S.; Zyryanov, G.V.; Ranu, B.C. Polymers and polymer-based materials for the detection of (nitro-)explosives. *Materials* **2023**, *16*, 6333. [[CrossRef](#)]
3. Li, L.; Bi, X.; Zhen, M.; Ren, Y.; Zhang, L.; You, T. Recent advances in analytical sensing detection of heavy metal ions based on covalent organic frameworks nanocomposites. *TrAC Trends Anal. Chem.* **2024**, *171*, 117488. [[CrossRef](#)]
4. Li, T.; Shao, Y.; Zhang, S.; Qin, J.; Fan, L.; Liu, L.; Wang, B.; Yang, Z.; Wang, Y. Two dinuclear Zn(II) complexes for the fluorescent detection of 2,4,6-trinitrophenol. *J. Lumin.* **2017**, *181*, 345–351. [[CrossRef](#)]
5. Agarwal, A.; Bhatta, R.P.; Kachwal, V.; Laskar, I.R. Controlling the sensitivity and selectivity for the detection of nitro-based explosives by modulating the electronic substituents on the ligand of AIPE-active cyclometalated iridium(III) complexes. *Dalton Trans.* **2023**, *52*, 14182–14193. [[CrossRef](#)]
6. Lin, L.; Rong, M.; Lu, S.; Song, X.; Zhong, Y.; Yan, J.; Wang, Y.; Chen, X. A facile synthesis of highly luminescent nitrogen-doped graphene quantum dots for the detection of 2,4,6-trinitrophenol in aqueous solution. *Nanoscale* **2015**, *7*, 1872–1878. [[CrossRef](#)] [[PubMed](#)]
7. Nayab, P.S.; Shkir, M. A dual responsive colorimetric and fluorescent reversible turn-on chemosensor for iron (Fe³⁺): Computational and spectroscopic investigations. *Sens. Actuators B Chem.* **2017**, *245*, 395–405. [[CrossRef](#)]
8. Du, J.-L.; Zhang, X.-Y.; Li, C.-P.; Gao, J.-P.; Hou, J.-X.; Jing, X.; Mu, Y.-J.; Li, L.-J. A bi-functional luminescent Zn(II)-MOF for detection of nitroaromatic explosives and Fe³⁺ ions. *Sens. Actuators B Chem.* **2018**, *257*, 207–213. [[CrossRef](#)]
9. Çelik, G.G.; Şenkuytu, E.; Şahin, O.; Serin, S. The new water-soluble Schiff base derivative fluorometric chemosensor with highly selective and instantly sensitivity for Fe³⁺ ion detection in aqueous media. *Inorg. Chim. Acta* **2021**, *527*, 120556. [[CrossRef](#)]
10. Das, P.; Das, M.; Biswas, R.; Laha, S.; Samanta, B.C.; Maity, T. Morphological adaptability through structural alterations in an AIE active novel chemosensor with Al(III), Fe(III), and gas phase/aqueous phase TNP recognition ability. *New J. Chem.* **2024**, *48*, 5820–5833. [[CrossRef](#)]
11. Zhang, Y.; Wang, G.; Zhang, J. Study on a highly selective fluorescent chemosensor for Fe³⁺ based on 1,3,4-oxadiazole and phosphonic acid. *Sens. Actuators B Chem.* **2014**, *200*, 259–268. [[CrossRef](#)]
12. Kagit, R.; Yildirim, M.; Ozay, O.; Yesilot, S.; Ozay, H. Phosphazene based multicentered naked-eye fluorescent sensor with high selectivity for Fe³⁺ ions. *Inorg. Chem.* **2014**, *53*, 2144–2151. [[CrossRef](#)]
13. Zhu, X.; Duan, Y.; Li, P.; Fan, H.; Han, T.; Huang, X. A highly selective and instantaneously responsive Schiff base fluorescent sensor for the “turn-off” detection of iron(III), iron(II), and copper(II) ions. *Anal. Methods* **2019**, *11*, 642–647. [[CrossRef](#)]
14. Liu, W.; Yang, H.; Zhang, Y. A two-fold interpenetrated 2D Zn (II) coordination polymer for sensitive and stable sensing of Fe³⁺/nitrofurantoin. *Polyhedron* **2024**, *248*, 116775. [[CrossRef](#)]
15. Ma, D.-L.; Lin, S.; Wang, W.; Yang, C.; Leung, C.-H. Luminescent chemosensors by using cyclometalated iridium(III) complexes and their applications. *Chem. Sci.* **2017**, *8*, 878–889. [[CrossRef](#)] [[PubMed](#)]
16. Kang, T.-S.; Zhang, J.-T.; Vellaisamy, K.; Ma, D.-L.; Leung, C.-H. Recent progress and developments of iridium-based compounds as probes for environmental analytes. *Dalton Trans.* **2018**, *47*, 13314–13317. [[CrossRef](#)]
17. Jing, S.; Wu, X.; Niu, D.; Wang, J.; Leung, C.-H.; Wang, W. Recent advances in organometallic NIR iridium(III) complexes for detection and therapy. *Molecules* **2024**, *29*, 256. [[CrossRef](#)] [[PubMed](#)]
18. Gao, H.; Qian, M.; Yang, X.; Ma, S.; Li, H. Recent advances of the cyclometalated iridium(III) complexes for electrochemiluminescence sensing. *Dyes Pigm.* **2025**, *232*, 112493. [[CrossRef](#)]
19. Manimaran, B.; Thanasekaran, P.; Rajendran, T.; Lin, R.-J.; Chang, I.-J.; Lee, G.-H.; Peng, S.-M.; Rajagopal, S.; Lu, K.-L. Luminescence enhancement induced by aggregation of alkoxy-bridged rhenium(I) molecular rectangles. *Inorg. Chem.* **2002**, *41*, 5323–5325. [[CrossRef](#)]
20. Shan, G.-G.; Zhang, L.-Y.; Li, H.-B.; Wang, S.; Zhu, D.-X.; Li, P.; Wang, C.-G.; Su, Z.-M.; Liao, Y. A cationic iridium(III) complex showing aggregation-induced phosphorescent emission (AIPE) in the solid state: Synthesis, characterization and properties. *Dalton Trans.* **2012**, *41*, 523–530. [[CrossRef](#)]
21. Shen, W.; Yan, L.; Tian, W.; Cui, X.; Qi, Z.; Sun, Y. A novel aggregation induced emission active cyclometalated Ir(III) complex as a luminescent probe for detection of copper(II) ion in aqueous solution. *J. Lumin.* **2016**, *177*, 299–305. [[CrossRef](#)]
22. Chao, D.; Zhang, Y. A water-soluble cationic Ir(III) complex for turn-on sensing of ClO₄[−] based on aggregation-induced emission. *Sens. Actuators B Chem.* **2017**, *245*, 599–604. [[CrossRef](#)]

23. Di, L.; Xing, Y.; Yang, Z.; Xia, Z. Ultrabright AIE of Ir(III) complexes achieving expeditious monitoring of oxygen and high-definition development of latent fingerprints. *Sens. Actuators B Chem.* **2022**, *350*, 130894. [[CrossRef](#)]
24. Yang, C.; Wen, L.-L.; Shan, G.-G.; Sun, H.-Z.; Mao, H.-T.; Zhang, M.; Su, Z.-M. Di-/trinuclear cationic Ir(III) complexes: Design, synthesis and application for highly sensitive and selective detection of TNP in aqueous solution. *Sens. Actuators B Chem.* **2017**, *244*, 314–322.
25. Che, W.; Li, G.; Liu, X.; Shao, K.; Zhu, D.; Su, Z.; Bryce, M.R. Selective sensing of 2,4,6-trinitrophenol (TNP) in aqueous media with “aggregation-induced emission enhancement” (AIEE)-active iridium(III) complexes. *Chem. Commun.* **2018**, *54*, 1730–1733. [[CrossRef](#)] [[PubMed](#)]
26. Liu, J.-W.; Xu, Y.-N.; Qin, C.-Y.; Wang, Z.-N.; Wu, C.-J.; Li, Y.-H.; Wang, S.; Zhang, K.Y.; Huang, W. Simple fluorene oxadiazole-based Ir(III) complexes with AIPE properties: Synthesis, explosive detection and electroluminescence studies. *Dalton Trans.* **2019**, *48*, 13305–13314. [[CrossRef](#)] [[PubMed](#)]
27. Dong, W.; Ma, Q.; Ma, Z.; Duan, Q.; Lü, X.; Qiu, N.; Fei, T.; Su, Z. Phosphorescent iridium(III) complex based photoluminescence sensor for sensitive and selective detection of picric acid. *Dyes Pigm.* **2020**, *172*, 107799. [[CrossRef](#)]
28. Hou, X.-G.; Wu, Y.; Cao, H.-T.; Sun, H.-Z.; Li, H.-B.; Shan, G.-G.; Su, Z.-M. A cationic iridium(III) complex with aggregation-induced emission (AIE) properties for highly selective detection of explosives. *Chem. Commun.* **2014**, *50*, 6031–6034. [[CrossRef](#)] [[PubMed](#)]
29. Sathish, V.; Ramdass, A.; Velayudham, M.; Lu, K.-L.; Thanasekaran, P.; Rajagopal, S. Development of luminescent sensors based on transition metal complexes for the detection of nitroexplosives. *Dalton Trans.* **2017**, *46*, 16738–16769. [[CrossRef](#)] [[PubMed](#)]
30. Shi, Y.-S.; Yu, Q.; Zhang, J.-W.; Cui, G.-H. Four dual-functional luminescent Zn(II)-MOFs based on 1,2,4,5-benzenetetracarboxylic acid with pyridylbenzimidazole ligands for detection of iron(III) ions and acetylacetone. *CrystEngComm* **2021**, *23*, 1604–1615. [[CrossRef](#)]
31. Zhang, Y.-T.; Ruan, J.-X.; Ma, D.-S.; Gao, J.-S.; Liu, Y.-F.; Yu, Y.-H. Two series of luminescent phosphonate coordination polymers of lanthanides for sensing ketones and Fe³⁺ in water. *Polyhedron* **2022**, *216*, 115694. [[CrossRef](#)]
32. Li, Z.; Hou, J.-T.; Wang, S.; Zhu, L.; He, X.; Shen, J. Recent advances of luminescent sensors for iron and copper: Platforms, mechanisms, and bio-applications. *Coord. Chem. Rev.* **2022**, *469*, 214695. [[CrossRef](#)]
33. Temram, T.; Klaimanee, E.; Saithong, S.; Amornpitoksuk, P.; Phongpaichit, S.; Ratanaphan, A.; Tantirungrotechai, Y.; Leesakul, N. Iridium(III) complexes based on cyanomethane and cyanamide ligands with luminescence quenching properties for Fe(III) sensing and biological activities. *Polyhedron* **2023**, *243*, 116540. [[CrossRef](#)]
34. Yan, Y.; Jia, W.; Zhang, L.; Liu, C. Fluorophenyl-modified AIPE-active cationic Pt(II) complexes for detecting picric acid in aqueous media. *Dyes Pigm.* **2023**, *220*, 111719. [[CrossRef](#)]
35. Yan, Y.; Jia, W.; Cai, R.; Liu, C. An AIPE-active fluorinated cationic Pt(II) complex for efficient detection of picric acid in aqueous media. *Chin. Chem. Lett.* **2024**, *35*, 108819. [[CrossRef](#)]
36. Zhang, Q.; Yan, Y.; Cai, R.; Li, X.-N.; Liu, C. Diphenylamino-modified neutral Pt(II) complexes: Their aggregation-induced phosphorescent emission and picric acid-sensing properties. *Materials* **2024**, *17*, 4366. [[CrossRef](#)] [[PubMed](#)]
37. He, P.; Chen, Y.; Li, X.-N.; Yan, Y.-Y.; Liu, C. Aggregation-induced emission-active iridium(III) complexes for sensing picric acid in water. *Chemosensors* **2023**, *11*, 177. [[CrossRef](#)]
38. Xu, J.; Zhang, L.; Shi, Y.; Liu, C. Carbazolyl-modified neutral Ir(III) complexes for efficient detection of picric acid in aqueous media. *Sensors* **2024**, *24*, 4074. [[CrossRef](#)] [[PubMed](#)]
39. Chen, Y.; Shi, Y.; Gao, Z.; Wang, L.; Tang, Y.; Liu, J.; Liu, C. Supramolecular copolymers under kinetic, thermodynamic, or pathway-switching control. *Angew. Chem. Int. Ed.* **2023**, *62*, e202302581. [[CrossRef](#)]
40. Chen, Y.; Wan, Q.; Shi, Y.; Tang, B.; Che, C.-M.; Liu, C. Three-component multiblock 1D supramolecular copolymers of Ir(III) complexes with controllable sequences. *Angew. Chem. Int. Ed.* **2023**, *62*, e202312844. [[CrossRef](#)] [[PubMed](#)]
41. Fan, C.; Li, Y.; Yang, C.; Wu, H.; Qin, J.; Cao, Y. Phosphoryl/sulfonyl-substituted iridium complexes as blue phosphorescent emitters for single-layer blue and white organic light-emitting diodes by solution process. *Chem. Mater.* **2012**, *24*, 4581–4587. [[CrossRef](#)]
42. Yun, H.-J.; Kim, K.-H.; Kang, S.-H.; Kim, J.-J.; Kim, Y.-H. Deep-blue phosphorescent emitters with phosphoryl groups for organic light-emitting diodes by solution processes. *Isr. J. Chem.* **2014**, *54*, 993–998. [[CrossRef](#)]
43. Yi, C.; Tian, W.; Song, B.; Zheng, Y.; Qi, Z.; Qi, Q.; Sun, Y. A new turn-off fluorescent chemosensor for iron (III) based on new diphenylfluorenes with phosphonic acid. *J. Lumin.* **2013**, *141*, 15–22. [[CrossRef](#)]
44. Verma, T.; Verma, P.; Singh, U.P. A multi responsive phosphonic acid based fluorescent sensor for sensing Fe³⁺, benzaldehyde and antibiotics. *Microchem. J.* **2023**, *191*, 108771. [[CrossRef](#)]
45. Yu, H.; Liu, C.; Lv, X.; Xiu, J.; Zhao, J. Effect of substituents on properties of diphenylphosphoryl-substituted bis-cyclometalated Ir(III) complexes with a picolinic acid as ancillary ligand. *Dyes Pigm.* **2017**, *145*, 136–143. [[CrossRef](#)]

46. Chuvashov, R.D.; Zhilina, E.F.; Lugovik, K.I.; Baranova, A.A.; Khokhlov, K.O.; Belyaev, D.V.; Eddin, M.Z.; Rusinov, G.L.; Verbitskiy, E.V.; Charushin, V.N. Trimethylsilylethynyl-substituted pyrene doped materials as improved fluorescent sensors towards nitroaromatic explosives and related compounds. *Chemosensors* **2023**, *11*, 167. [[CrossRef](#)]
47. Ouyang, T.; Guo, X.; Cui, Q.; Zhang, W.; Dong, W.; Fei, T. Conjugated polymer nanoparticles based on anthracene and tetraphenylethene for nitroaromatics detection in aqueous phase. *Chemosensors* **2022**, *10*, 366. [[CrossRef](#)]
48. Zu, F.; Yan, F.; Bai, Z.; Xu, J.; Wang, Y.; Huang, Y.; Zhou, X. The quenching of the fluorescence of carbon dots: A review on mechanisms and applications. *Microchim. Acta* **2017**, *184*, 1899–1914. [[CrossRef](#)]
49. Thippeswamy, M.S.; Naik, L.; Maridevarmath, C.V.; Savanur, H.M.; Malimath, G.H. Studies on the characterisation of thiophene substituted 1,3,4-oxadiazole derivative for the highly selective and sensitive detection of picric acid. *J. Mol. Struct.* **2022**, *1264*, 133274. [[CrossRef](#)]
50. Li, Z.; Li, H.; Shi, C.; Yu, M.; Wei, L.; Ni, Z. Nanomolar colorimetric quantitative detection of Fe³⁺ and PPI with high selectivity. *Spectrochim. Acta Part A* **2016**, *159*, 249–253. [[CrossRef](#)] [[PubMed](#)]
51. Elmas, S.N.K.; Karagoz, A.; Arslan, F.N.; Yilmaz, I. Propylimidazole functionalized coumarin derivative as dual responsive fluorescent chemoprobe for picric acid and Fe³⁺ recognition: DFT and natural spring water applications. *J. Fluoresc.* **2022**, *32*, 1357–1367. [[CrossRef](#)] [[PubMed](#)]

Disclaimer/Publisher's Note: The statements, opinions and data contained in all publications are solely those of the individual author(s) and contributor(s) and not of MDPI and/or the editor(s). MDPI and/or the editor(s) disclaim responsibility for any injury to people or property resulting from any ideas, methods, instructions or products referred to in the content.